Environ Sci Pollut Res (2017) 24:1926–1937
DOI 10.1007/s11356-016-7866-8

RESEARCH ARTICLE

Magnetically separable maghemite/montmorillonite composite as an efficient heterogeneous Fenton-like catalyst for phenol degradation

Mingjie Jin[1] · Mingce Long[2,3] · Hanrui Su[2] · Yue Pan[2] · Qiuzhuo Zhang[4] · Juan Wang[4] · Baoxue Zhou[2,3] · Yanwu Zhang[1]

Received: 16 June 2016 / Accepted: 7 October 2016 / Published online: 31 October 2016
© Springer-Verlag Berlin Heidelberg 2016

Abstract To develop highly efficient and conveniently separable iron containing catalysts is crucial to remove recalcitrant organic pollutants in wastewater through a heterogeneous Fenton-like reaction. A maghemite/montmorillonite composite was synthesized by a coprecipitation and calcination method. The physiochemical properties of catalysts were characterized by XRD, TEM, nitrogen physisorption, thermogravimetric analysis/differential scanning calorimetry (TG/DSC), zeta potential, and magnetite susceptibility measurements. The influence of calcination temperatures and reaction parameters was investigated. The calcined composites retain magnetism because the presence of montmorillonite inhibited the growth of γ-Fe_2O_3 nanoparticles, as well as their phase transition. The catalytic activities for phenol degradation were significantly enhanced by calcinations, which strengthen the interaction between iron oxides and aluminosilicate framework and result in more negatively charged surface. The composite (73 m^2/g) calcined at 350 °C had the highest catalytic activities, with more than 99 % phenol reduction after only 35 min reaction at pH 3.6. Simultaneously, this catalyst exhibited high stability, low iron leaching, and magnetically separable ability for consecutive usage, making it promising for the removal of recalcitrant organic pollutants in wastewater.

Keywords Heterogeneous Fenton-like reaction · Maghemite · Montmorillonite · Magnetic separable · Phenol degradation · Wastewater

Responsible editor: VÃtor Pais Vilar

Electronic supplementary material The online version of this article (doi:10.1007/s11356-016-7866-8) contains supplementary material, which is available to authorized users.

✉ Mingce Long
Long_mc@sjtu.edu.cn

✉ Yanwu Zhang
zhangyanwu@zzu.edu.cn

[1] School of Chemical Engineering and Energy, Zhengzhou University, Zhengzhou 450001, China

[2] School of Environmental Science and Engineering, Shanghai Jiao Tong University, Shanghai 200240, China

[3] Key Laboratory for Thin Film and Microfabrication of the Ministry of Education, Shanghai Jiao Tong University, 800 Dong Chuan Road, Shanghai 200240, China

[4] School of Ecological and Environmental Sciences, East China Normal University, Shanghai 200241, China

Introduction

With the increase of industry production and the improvement of living standards, it is currently inevitable to discharge wastewater containing recalcitrant organic pollutants. Among those organic contaminants, phenolic compounds have gained much attention due to their wide applications in industry and hazard to human central nervous system and kidneys (Bruce et al. 2001; Iurascu et al. 2009; Xu and Wang 2011). The tolerable intake of phenol has been determined as 120 μg/kg body weight per day (Bruce et al. 2001). According to the integrated wastewater discharge standard of Shanghai Municipal, the maximum dischargeable concentration of phenol, listed as the class 2 hazard pollutants in wastewater, is 0.5 mg/L. Unfortunately, traditional treatment methods, such as physiochemical separation, chemical oxidation, and biological degradation, would be hard to meet such a strict standard. High cost and prolonged treating time frequently hindered in the treatment of phenolic compounds containing wastewater. Therefore, cost-efficient wastewater treatment technologies are still urgently demanded.

Heterogeneous Fenton-like reaction, as a type of advanced oxidation technology that uses iron or other metal containing materials (e.g., Fe_2O_3, Fe_3O_4, FeOOH, etc.) as catalysts for the activation of H_2O_2 and production of hydroxyl radicals, has stimulated increasing interests due to such advantages as relatively wider working pH, without iron sludge pollution, and acceptable cost (Lin and Gurol 1998; Oliveira et al. 2012; Pham et al. 2009; Usman et al. 2012; Xia et al. 2011b; Zhang et al. 2009). Although iron containing compounds or materials can be directly used, their catalytic activities for H_2O_2 activation and organic degradation are not satisfactory (Djeffal et al. 2014; Usman et al. 2012, 2013). Immobilizing iron oxides on smectite clay is a promising strategy to further improve their performance in degradation of recalcitrant organic pollutants (Chen and Zhu 2007, 2011; Chen et al. 2010; Feng et al. 2004, 2006; Garrido-Ramirez et al. 2010; Iurascu et al. 2009; Virkutyte and Varma 2014; Zhang et al. 2010). Smectite clay, a class of layered aluminosilicates, is a promising benign material and widely applied in environmental restoration and remediation. Moreover, the intercalated metal oxides in clays would not only introduce the active sites for H_2O_2 activation but also prevent the collapse of interlayer spaces and generate larger micropores (Chae et al. 2001).

Magnetically separable superparamagnetic materials, such as Fe_3O_4 or γ-Fe_2O_3, enabling nanomaterials the property of facile separation and recycling by external magnetic field (Kalidasan et al. 2016; Wang et al. 2015; Yu et al. 2014), have become popular components of adsorbents or catalysts in wastewater treatment applications (Ling et al. 2014; Lou et al. 2015; Qin et al. 2014; Munoz et al. 2015). However, as heterogeneous Fenton catalysts, they are always suffering from low catalytic activities and instabilities. Fe_3O_4 can be slowly oxidized in aerobic conditions, while metastable maghemite (γ-Fe_2O_3) would transform into hematite (α-Fe_2O_3) upon calcinations above 250 °C (Herrero et al. 1997; Schimanke and Martin 2000). In most cases, calcinations are frequently applied in catalyst syntheses to remove defects and bounded water and accordingly influence the catalytic performance. Therefore, how to develop highly efficient catalysts for H_2O_2 activation and simultaneously retain the magnetic property after calcinations is one of crucial challenges. Magnetic separable montmorillonite/bentonite composites have been frequently investigated as adsorbents (Lou et al. 2015; Zhang et al. 2016) or catalysts (Li et al. 2016; Wan et al. 2015; Virkutyte and Varma 2014). However, there are a very few reports on γ-Fe_2O_3-based smectite clays for heterogeneous Fenton applications (Virkutyte and Varma 2014; Tireli et al. 2015). Virkutyte et al. have reported a γ-Fe_2O_3-pillared montmorillonite for heterogeneous catalytic activation oxone, peracetic acid, and hydrogen peroxide. However, it is not clear about the magnetic properties and the influence of calcination temperatures, and the catalytic activity for H_2O_2 activation should be further improved.

In this paper, a magnetically separable maghemite/montmorillonite catalyst has been developed through a coprecipitation and calcination method. This catalyst displayed the retained magnetic performance and a highly efficient catalytic activity for phenol degradation without any energy input or additives. The corresponding mechanisms on the formation chemistry and the enhanced catalytic activity upon calcination were investigated.

Materials and methods

Materials

Ferric chloride ($FeCl_3 \cdot 6H_2O$), hydrogen peroxide (H_2O_2, 30 wt%), and phenol (C_6H_6O) were purchased from Sinopharm Chemical Reagent Co., Ltd. Ferrous chloride ($FeCl_2 \cdot 4H_2O$) was obtained from Aladdin Chemistry Co., Ltd. Montmorillonite K10 (MK10) was procured from Sigma-Aldrich (Germany). HPLC-grade methanol was obtained from Fisher Scientific Company (Fair Lawn, USA). All other chemicals were of analytical grade and used without further purification.

Syntheses of catalysts

$FeCl_2 \cdot 4H_2O$ (5.652 g) and $FeCl_3 \cdot 6H_2O$ (3.841 g) were dissolved in 80 mL deionized water, and then 4 g MK10 was added into the solution. The mixture was stirred under N_2 atmosphere at 90 °C for 30 min. Then, 40 mL ammonium hydroxide (25 wt%) was injected into the mixture, which was stirred for another 60 min to complete the reaction. After cooling, the magnetic composites (Fe_3O_4/MK10) were filtered and washed three times with deionized water. Finally, the obtained Fe_3O_4/MK10 was dried at 60 °C (named as IB-60) and calcined in a muffle furnace for 24 h at various temperatures (denoted as IB-T, in which T is the calcination temperature). Meanwhile, Fe_3O_4 nanoparticle was synthesized by the same method but without MK10, which was designated as IO-60. The corresponding calcined IO-60 samples at various temperatures were designated as IO-T.

Characterization methods

The crystalline phase of composites was identified by a Rigaku D/max-2200/PC X-ray diffraction (XRD) instrument with Cu Kα radiation. Samples were scanned at 2θ from 10° to 80°. X-ray photoelectron spectroscopy (XPS) measurements were carried out on an Axis Ultra DLD system (Kratos Ltd., Japan). The morphology of samples was observed with a transmission electron microscope (TEM, H-7500, Hitachi, Japan). The Brunauer-Emmett-Teller (BET) surface areas and pore size distributions of samples

were carried out using a Quantachrome NOVA 2200e system with N_2 as the adsorption gas. Thermogravimetric (TG) and differential scanning calorimetry (DSC) curves were measured using a Mettler Toledo (Switzerland) analyzer at a heating rate of 10 °C/min in air from 20 to 460 °C. The magnetite susceptibility measurements were carried out on a physical property measurement system (PPMS-9T, Quantum Design, USA). The surface charges of catalysts and particle sizes of MK10 were obtained by a particle size and zeta potential analyzer (Delsa Nano C, Beckman Coulter, USA) in aqueous media at different pH values. Total organic carbon (TOC) was measured by a TOC/TN analyzer (Multi 3100, Analytic Jena, Germany).

Catalytic performance

A series of batch experiments of phenol degradation in suspensions were carried out to evaluate the catalytic activity of synthesized catalysts. In a typical test, 0.02 g of catalyst was added into a phenol solution (20 mL, 100 mg/L) in a 25-mL conical flask, and the initial pH was adjusted to 3.6 by adding drops of 1 M NaOH or HNO_3. The flasks were kept stirring at a mild temperature (30 °C) for 20 min to achieve adsorption equilibrium. Then, a certain amount of H_2O_2 was added. At a fixed interval, 0.5 mL sample was withdrawn and filtered into a vial with 0.5 mL methanol to quench the reaction. The aqueous phase was sampled for the analyses of phenol concentrations, pH, and total soluble ferric ions. Phenol and its degradation intermediates were analyzed by a high performance liquid chromatography (HPLC-2010A, Shimadzu) with a Shim Pack C18 chromatographic column. Elution was carried out with a 70:30 (*v*/*v*) mixture of methanol and aqueous H_3PO_4 (0.1 wt%) at a 0.9-mL/min flow rate. The detection wavelength was 270 nm. Total dissolved iron concentration in the suspension was measured according to the 1,10-phenanthroline method on a UV–VIS spectrophotometer (WFJ-7200, UNIC) (Tamura et al. 1974). The remaining H_2O_2 in reaction solutions was measured according to a metavanadate method (Ling et al. 2014; Nogueira et al. 2005).

Results and discussion

Physicochemical characterizations

The XRD patterns of MK10 and catalysts are shown in Fig. 1. All diffraction peaks of MK10 could be attributed to those of typical quartz (JCPDS No. 86-1560) and montmorillonite (JCPDS No. 3-0016) (Lou et al. 2015). Besides these diffraction peaks, the black IB-60 powder shows other additional diffraction peaks at 30.0°, 35.3°, 43.0°, 53.4°, 56.9°, and 62.5°, which correspond to (2 2 0), (3 1 1), (4 0 0), (4 2 2), (5 1 1), and (4 4 0) planes of Fe_3O_4 in a cubic phase (JCPDS No. 19-0629) (Zhou et al. 2014a, b), indicating IB-60 is a composite of Fe_3O_4 and MK10. There is no other peak associating to $Fe(OH)_3$ or α-Fe_2O_3, which are usual by-products in the coprecipitation procedure (Jiang et al. 2004). It is interesting that the diffraction patterns of all IB-T samples are almost the same as its precursor IB-60, even after calcined at a temperature as high as 450 °C for as long as 24 h. However, the color of catalysts changes from black to red after calcined above 180 °C, suggesting a phase transition from Fe_3O_4 to γ-Fe_2O_3 (JCPDS No. 4-0755). Although both two phases have the same XRD diffraction patterns, the phase transition can be further discerned by their XPS spectra (Fig. S1). Compared with IB-60, the satellite peak at around 718.0 eV in the Fe 2p spectrum of IB-180 is attributed to γ-Fe_2O_3 (Gao et al. 2013; Grosvenor et al. 2004; Yamashita and Hayes 2008).

According to XRD patterns in Fig. 1b, the control sample IO-60 is a typical Fe_3O_4 in a cubic phase, while IO-350 is a mixture of maghemite (γ-Fe_2O_3) and hematite (α-Fe_2O_3), and they have completely transformed into hematite in IO-450. Those diffraction peaks discernible in the XRD pattern of IO-450 at 24.1°, 33.1°, 40.9°, and 49.5° correspond to (0 1 2), (1 0 4), (1 1 3), and (0 2 4) planes of α-Fe_2O_3 (JCPDS No. 33-0664), respectively (Cao et al. 2015; Orolinova et al. 2012). Moreover, the relative intensity variation of characteristic reflections of IB-T and IO-T in Fig. S2 describes the phase transition clearly. The ratios of (2 2 0), (3 1 1), (4 4 0), and (5 1 1) reflection intensities of γ-Fe_2O_3 for calcined IB-T to those of Fe_3O_4 for IB-60 were plotted as a function of

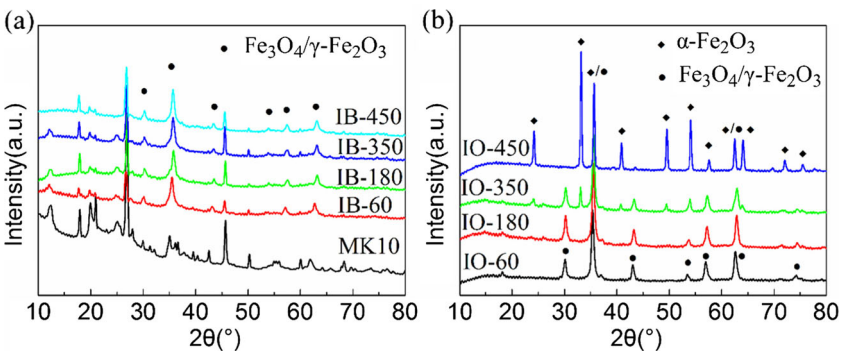

Fig. 1 XRD patterns: **a** MK10 and IB-T and **b** IO-T

calcined temperatures (Fig. S2a). There is no obvious change in the intensity ratios at the temperatures below 450 °C, indicating negligible phase transition of γ-Fe_2O_3. The ratios of (0 1 2), (1 0 4), (1 1 3), and (0 2 4) reflection intensities of α-Fe_2O_3 for IO-T to those for IO-450 were also plotted in Fig. S2b. The positive data of ratios suggest the appearance of α-Fe_2O_3. As a result of the phase transition from maghemite to hematite, the ratios increase sharply after calcined above 350 °C. This result is consistent with previous reports that maghemite would easily transform into hematite upon calcinations (Herrero et al. 1997; Machala et al. 2011; Schimanke and Martin 2000).

The average crystallite sizes are estimated from the width of the most remarkable diffraction peak using Debye-Scherrer formula (Eq. 1).

$$d = \frac{k\lambda}{\beta\cos(\theta)} \quad (1)$$

wherein d is the diameter of the particle, k (0.89) is the Debye-Scherrer constant, λ (0.154 nm) is the wavelength of X-ray irradiation, β is the full width at half maximum (FWHM) value of XRD diffraction lines, and θ is the scattering angle. The temperature dependence of average crystallite sizes calculated according to the (3 1 1) diffraction peak of γ-Fe_2O_3 or (1 1 0) of α-Fe_2O_3 is shown in Fig. 2. As expectation, the calculated sizes of catalysts are positively related with calcination temperatures. It is obvious that the sizes of IO-T dramatically grow up at higher temperatures. The average diameter of nanoparticles almost doubles from 16.87 nm for IO-60 to 31.91 nm for IO-450. However, in the presence of layered clay, the growth of iron oxide crystallites in the composites is significantly hindered. The sizes of iron oxides change from 10.32 nm for IB-60 to only 13.32 nm for IB-450. It has been reported that upon calcinations the phase transition of γ-Fe_2O_3 could take place quickly once the size of γ-Fe_2O_3 nanoparticles reached a certain critical value (usually between 20 and 25 nm) (Machala et al. 2011; Schimanke and Martin 2000). Therefore, in the absence of montmorillonite, γ-Fe_2O_3 in IO-180 transforms into α-Fe_2O_3 easily when calcined at above 350 °C, and the phase transition completes after calcined at 450 °C for 24 h. Moreover, IO-450 lose magnetism due to the disappearance of γ-Fe_2O_3. However, all IB-T samples retain magnetism, and the presence of MK10 in IB-T composites inhibits the phase change of γ-Fe_2O_3, which could be attributed to the suppressed growth of iron oxide nanoparticles.

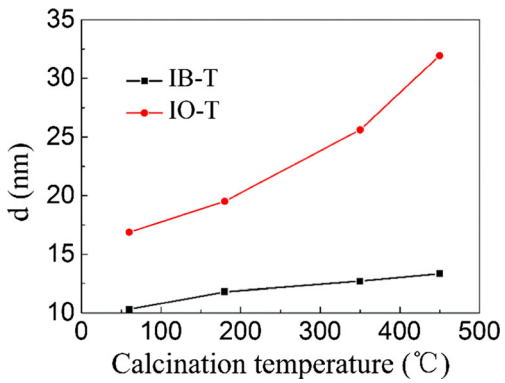

Fig. 2 The temperature dependence of crystalline sizes for IB-T and IO-T

The average particle size of MK10 was determined to be ~0.8 μm according to a dynamic light scattering method. The microscopic morphology of catalysts IO-60, IO-350, and IB-350 is shown in Fig. 3. Fe_3O_4 nanoparticles in IO-60 exhibit serious agglomeration, with an average diameter of 15–20 nm (Fig. 3a). The sizes of nanoparticles have obviously grown up into about 25–30 nm after calcined at 350 °C, with a more significant aggregation (Fig. 3b). However, in the composite IB-350, iron oxide nanoparticles dispersing on the layered MK10 show better uniformity, with an average diameter of 10–15 nm (Fig. 3c). These results are in accordance with those of XRD patterns.

Nitrogen adsorption–desorption isotherms (Fig. 4) and pore size distributions (Fig. S3) were measured for MK10 and catalysts. The BET method and Barrett-Joyner-Halenda (BJH) model were used to calculate specific surface area and porosity of catalysts, respectively. Results are summarized in Table 1. According to the IUPAC classification, all the samples exhibit type IV N_2 adsorption isotherms, indicating the presence of tiny capillary pores. When iron oxides immobilized on montmorillonite, the BET surface area decreased from 262 m^2/g for MK10 to 151 m^2/g for IB-60. After calcinations, BET surface areas of these nanocomposites showed a decreasing trend. Yet, IB-350 (73 m^2/g) possesses a notably higher BET surface area than that of IO-60 (22 m^2/g) or IO-350 (19 m^2/g). The high BET surface area of IB-350 can be attributed to the presence of substrate and the inhibited aggregation, which is favorable for adsorption and degradation of organic pollutants.

The physiochemical changes of MK10, IO-60, and IB-60 during calcinations were tracked by TG and DSC methods, as shown in Fig. 5. About 5.6, 8.4, and 0.6 % weight loss up to 200 °C for MK10, IB-60, and IO-60, accompanying with the endothermic peak in DSC curves, can be attributed to the loss of adsorbed water. It is interesting that weight loss of IB-60 is much higher than that of MK10, while that of IO-60 is very low, indicating that the IB-60 has a much stronger hydrophilic capability than others. Although the TG curve of IO-60 is horizontal from 200 to 460 °C, the obvious exothermic peak centered at 180 °C and another observable one at about 330 °C correspond to the occurrence of phase conversion from Fe_3O_4 to γ-Fe_2O_3 and then to α-Fe_2O_3, respectively. Both of these phase transitions are energy-released processes (Sanders and Gallagher 2003). The

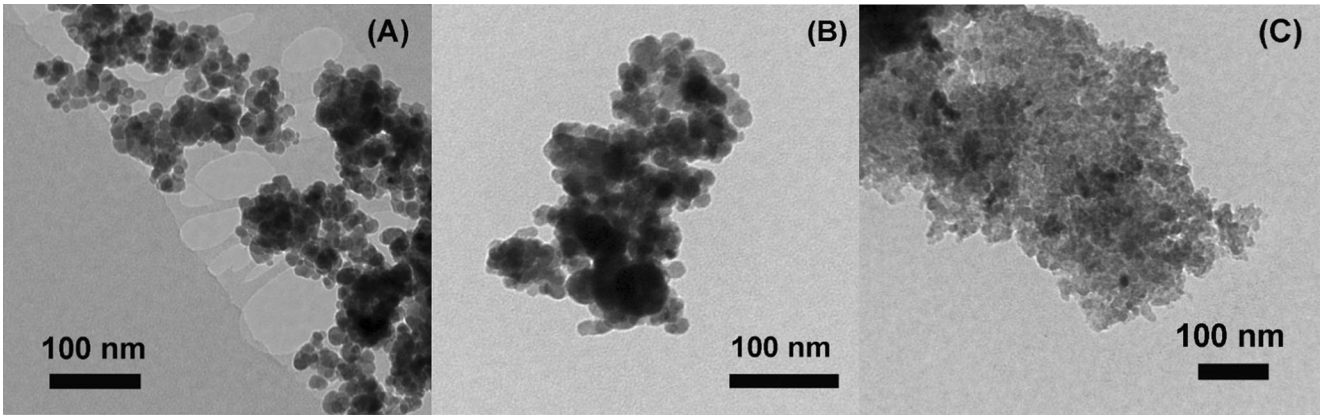

Fig. 3 TEM images of **a** IO-60, **b** IO-350, and **c** IB-350

recrystallization of montmorillonite would not take place below 600 °C (Sarikaya et al. 2000). The continuous weight losses in MK10 and IB-60 above 200 °C are caused mainly by the loss of bound water on the surface or in the pores of the layered clay. The slightly larger slope in the TG curve of IB-60 could be explained by that IB-60 has more bound water and larger pore sizes. However, the endothermic trend in the DSC curve of MK-10 above 300 °C is more significant than that of IB-60, although the later has much more losses of bound water. This suggests that the endothermic process of water loss in IB-60 has been partially balanced by the exothermic γ-Fe_2O_3 generation and uncertain exothermic interaction between iron oxides and the aluminosilicate framework of montmorillonite, which could also be supported by the lack of obvious exothermic peak above 200 °C in the DSC curve of IB-60. Therefore, upon calcinations of IB-60, besides the loss of adsorbed and bounded water, γ-Fe_2O_3 phase is generated and remained stable, and the interaction between both components in the composite could be further strengthened.

The magnetic properties of catalysts were measured on a physical property measurement system (PPMS) at a magnetic field in the range of −6000 to 6000 Oe, and the results of magnetic hysteresis curves are shown in Fig. 6. All catalysts possess a typical ferromagnetic hysteresis, corresponding to their strong response to magnetic field. The saturation magnetizations (Ms) of IO-60 and IO-350 are 65.16 and 45.61 emu/g, respectively. The significant decrease of Ms can be attributed to the emergence of α-Fe_2O_3. However, the values are comparable for IB-60 (13.84 emu/g) and IB-350 (12.81 emu/g), suggesting that those calcined at 350 °C have negligible influence on the magnetism of IB-60. Certainly, the presence of MK10 decreases Ms of the composite, but the value is comparable to other supported ferromagnetic catalysts (Ling et al. 2014; Xia et al. 2011a). The catalyst IB-350 can be easily separated from aqueous suspension using an external magnetic field (inset in Fig. 6), which would be greatly favorable for recycling of catalysts and reducing the cost in practical applications.

Catalytic performance for phenol degradation

Effect of calcination temperatures

Heterogeneous Fenton-like catalytic performance of these catalysts was explored through tracking the degradation of phenol in an aqueous suspension with the addition of H_2O_2. The reaction conditions are selected according to preliminary experiments: H_2O_2 dosage = 45 mmol/L, catalyst dosage = 1.0 g/L, initial pH = 3.6, temperature = 30 °C, and initial phenol concentration = 100 mg/L. Figure 7 shows the catalytic activities of various catalysts. IO-T samples display poor catalytic activities (Fig. 7a), with only 18.3, 11.7, 10.4, and 9.2 % phenol reduction after 120 min reaction for IO-60, IO-180, IO-350, and IO-450, respectively. Calcinations and phase transitions of iron oxides (IO-T) do not cause significant improvement in their catalytic activities. This could be attributed to the aggregation of particles, small surface area, and the

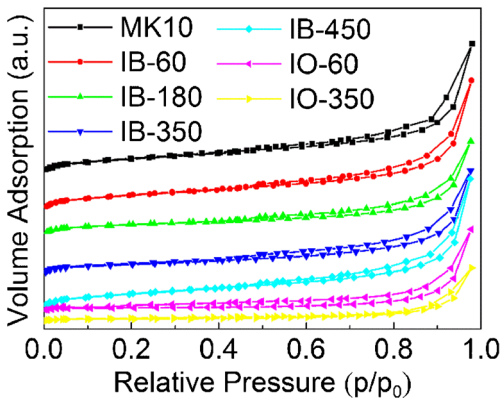

Fig. 4 Nitrogen adsorption isotherms of MK10 and catalysts

Table 1 BET surface areas, pore volumes, and pore sizes of samples

Sample	S_{BET} (m^2/g)	Pore diameter (nm)	Pore volume (cm^3/g)
MK10	262	3.64	0.30
IB-60	151	3.84	0.29
IB-180	102	3.83	0.21
IB-350	73	3.84	0.24
IB-450	84	3.84	0.18
IO-60	22	–	–
IO-350	19	–	–

appearance of α-Fe_2O_3, which possesses an even lower catalytic active than Fe_3O_4 and γ-Fe_2O_3.

It is interesting that the composites of IB-T display efficient catalytic activities for phenol degradation, and calcinations significantly improve their catalytic performance (Fig. 7b). After 120 min reaction, more than 99.9 % phenol reduction is achieved in the presence of IB-60. However, the control tests using IB-350 or H_2O_2 alone achieved only 4.9 or 10.1 % phenol reduction, suggesting that in the present conditions adsorption of phenol on IB-350 is negligible and H_2O_2 could not be activated without catalysts. The catalytic activity of IB-60 in H_2O_2 activation and phenol degradation could be attributed to the enhanced dispersion of Fe_3O_4 and the presence of MK10. In previous reports, it has been found that the interaction between Fe and oxides of Al or Si in the catalyst would result in a significantly enhancement of H_2O_2 activation (Pham et al. 2009). In MK10, as a kind of smectite clays, the percentages of Al and Si are determined as 45.6 and 11.2 wt%, respectively (Table S1). It can be expected that there is an interaction between Al or Si oxides in the clay and iron during the synthesis. More importantly, heat treatments significantly improve the catalytic performance. Although IB-350 has a relatively smaller BET surface area (73 m^2/g), it shows the highest catalytic activity, achieving more than 98.1 % phenol reduction after only 30 min reaction.

There are two possible reasons for the enhanced activities under calcinations. First, it can be expected that the interaction of Fe with Al or Si in the clay could be strengthened during calcinations, which is further supported by the changed zeta potentials of these catalysts (Fig. 8). Although their points of zero charge are approximation, the decreased tendencies above these points are quite different. This could be ascribed to that the interactions in IB-T were weakened and breached at low pH conditions. Zeta potential of IB-350 decreases sharply from −0.31 mV at pH 3.38 to −10.03 mV at pH 3.71. According to the tendencies, it can be anticipated that at the reaction pH, the order of zeta potentials for IB-T should be IB-350 < IB-450 < IB-180 < IB-1, which is the opposite of their catalytic performance. Generally, according to Haber-Weiss mechanism, the initial heterogeneous Fenton-like reaction can be described by Eqs. (2) and (3) (Lin and Gurol 1998; Pham et al. 2009). The former one was regarded as the rate-limiting step, because the kinetic rate constant for the transformation of Fe^{3+} into Fe^{2+} in the corresponding homogeneous reaction is very small (0.01–0.02 M^{-1} s^{-1}), which is about five orders of magnitude less than that for the second reaction (Chen and Pignatello 1997; Pham et al. 2009). Moreover, in the heterogeneous systems, adsorption of the electrophilic H_2O_2 on the active metal sites is required to initiate H_2O_2 decomposition (Du et al. 2006; Pham et al. 2009; Walling and Goosen 1973). Generally, on the one hand, negatively charged particle surface is favorable for the adsorption of H_2O_2 and accordingly helpful for the rate-limiting H_2O_2 decomposition in reaction (Pham et al. 2009; Xia et al. 2011b). On the other hand, the negative charged surface would also enable a proton concentrated layer over the surface and enhance the selectivity of H_2O_2 decomposition toward ·OH radicals (Xia et al. 2011b). Therefore, the highest catalytic activity of IB-350 could be attributed to the most negatively charged surface properties. Besides this, the strengthened interaction after extended calcinations would also change the density and the relative proximity of the reactive sites on the surface, which could also helpful to the redox cycle of ≡Fe(III)/≡Fe(II) (Pham et al. 2009). As IB-350 exhibits the highest catalytic activity in phenol degradation, it was selected for the further experiments.

$$\equiv Fe(III) + H_2O_2 \rightarrow \equiv Fe(II) + HO_2^{\cdot}\left(O_2^{-\cdot}\right) + H^+(2H^+) \quad (2)$$

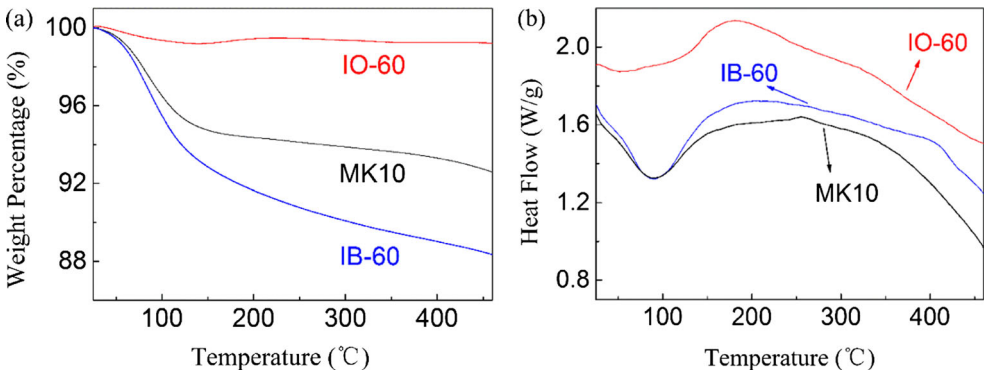

Fig. 5 TG (**a**) and DSC (**b**) curves of MK10, IB-60, and IO-60

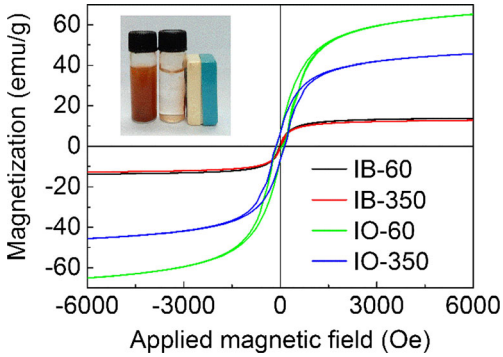

Fig. 6 Magnetic hysteresis curves of samples. *Inset*: photograph of magnetic separation of IB-350

$$\equiv Fe(II) + H_2O_2 \rightarrow \equiv Fe(III) + \ OH + OH^- \quad (3)$$

Effect of operating parameters

Effects of operating parameters, including the dosage of catalysts and H_2O_2, the initial pH, and phenol concentration, have been investigated and results are shown in Fig. 9. Removal of phenol was improved with the increase of catalyst dosages from 0.1 to 1.0 g/L (Fig. 9a). This is mainly attributed to that a higher catalyst dosage can provide more active sites to favor H_2O_2 activation and hydroxyl radical generation. However, when catalyst dosage further increased from 1.0 to 1.5 g/L, there was no observable increase of phenol reduction, which could be due to the saturation of active sites.

The effects of H_2O_2 dosage are shown in Fig. 9b. When H_2O_2 dosage increased from 15 to 45 mmol/L, phenol reduction in the first 30 min significantly improved from about 10.2 to 98.7 %. Generally, in a heterogeneous Fenton system, a higher H_2O_2 dosage than the theoretical value is used to achieve desirable reaction rates. This could be ascribed to the enhanced accessibility of H_2O_2 on the active sites, which would be favorable for the generation of active species. However, a further increase of H_2O_2 dosage (60 mmol/L) inhibited phenol degradation. This can be understood by the competition of radicals between H_2O_2 and phenol at a too high H_2O_2 concentration (Xia et al. 2011a, b).

The initial pH of reaction solution plays an important role for the ·OH production in both homogeneous and heterogeneous Fenton processes. Effect of pH was investigated by applying five different initial pH values. As shown in Fig. 9c, a lower pH was beneficial for the generation of ·OH, as well as the phenol degradation. More than 99 % phenol reduction can be achieved in only 20 min at an initial pH 3.2. However, too low pH would result in significant iron leaching. At near neutral pHs, the reaction rates were much slow, with only 28.6 and 14.1 % phenol reduction in 120 min at pH 5.0 and 6.0, respectively. This is consistent with previous results and could be due to the fact that H_2O_2 would rapidly decompose into molecular oxygen and H_2O at higher pHs (Xia et al. 2011a, b; Yu et al. 2015).

Generally, in a heterogeneous Fenton reaction, a higher pollutant initial concentration would result in a lower degradation efficiency. Figure 9d shows the effect of initial phenol concentration. It can be noted that phenol degradation rates decrease with the increase of initial concentrations. This could be ascribed to that phenol would compete active sites with H_2O_2. However, almost 100 % phenol reduction can be achieved after 120 min reaction even when its concentration increased to 200 mg/L.

Stability of the catalyst

To understand the chemical changes during phenol degradation and assess the stability of the catalyst, pH values and leached iron ions have been measured. As shown in Fig. 10, pH values of the suspension decrease slowly to 3.44 at the first 25 min and then sharply to 2.79 in the next 10 min,

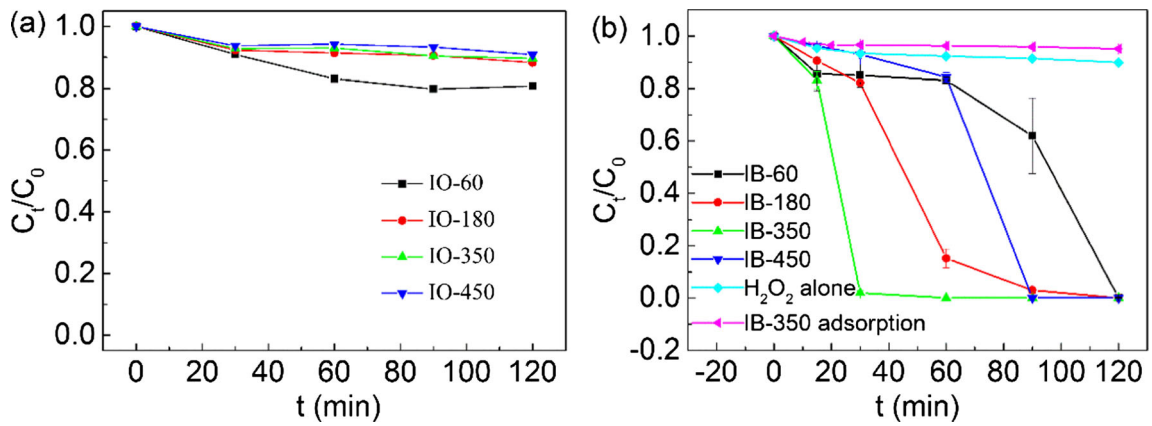

Fig. 7 Phenol degradation using different catalysts: **a** IO-T and **b** IB-T and control tests. (Initial pH = 3.6, 30 °C, 1.0 g/L catalyst, 100 mg/L phenol, and 45 mmol/L H_2O_2)

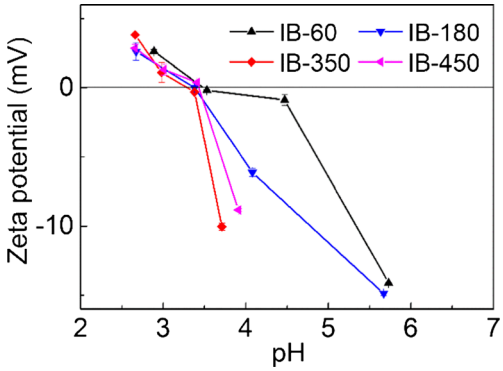

Fig. 8 Zeta potentials of IB-T as a function of pHs

accompanying with the fast phenol degradation. This can be ascribed to the generation of acidic intermediates, such as oxalic acid. Meanwhile, the concentration of total leached iron ions was measured to be only 0.01 mg/L after 25 min reaction. With the fast phenol degradation and pH decreases, the concentration of total dissolved iron ions increased to 0.072 mg/L after 35 min reaction. However, the leached percentage of iron is very low, only accounting for 0.02 % of iron in the catalysts. The contribution of homogeneous Fenton-like reaction caused by leached iron ions in the bulk solution was evaluated. The contrast experiment shows that phenol reduction is only 9.2 % after 35 min reaction in the presence of 0.072 mg/L iron ions ($FeCl_3$). Therefore, the contribution of homogeneous reaction is negligible, and the heterogeneous processes dominate in phenol degradation.

The stability of IB-350 was further evaluated by cycle tests and results are shown in Fig. 11. In each turn, used catalyst powder was magnetically separated from the reaction solution, washed by water, and dried at 60 °C for 5 h. The catalytic activity of IB-350 was reproducible in three consecutive experiments. Moreover, the leached iron ions in the three cycles after 35 min reactions were measured to be 0.072, 0.051, and 0.021 mg/L, respectively. The decreased concentration of leached iron ions is another piece of evidence for the high stability of this catalyst.

H_2O_2 utilization efficiency

TOC removal and H_2O_2 consumption during phenol degradation using IB-350 as a catalyst were tracked in Fig. 12. Their shapes are similar to the change of phenol concentration. After

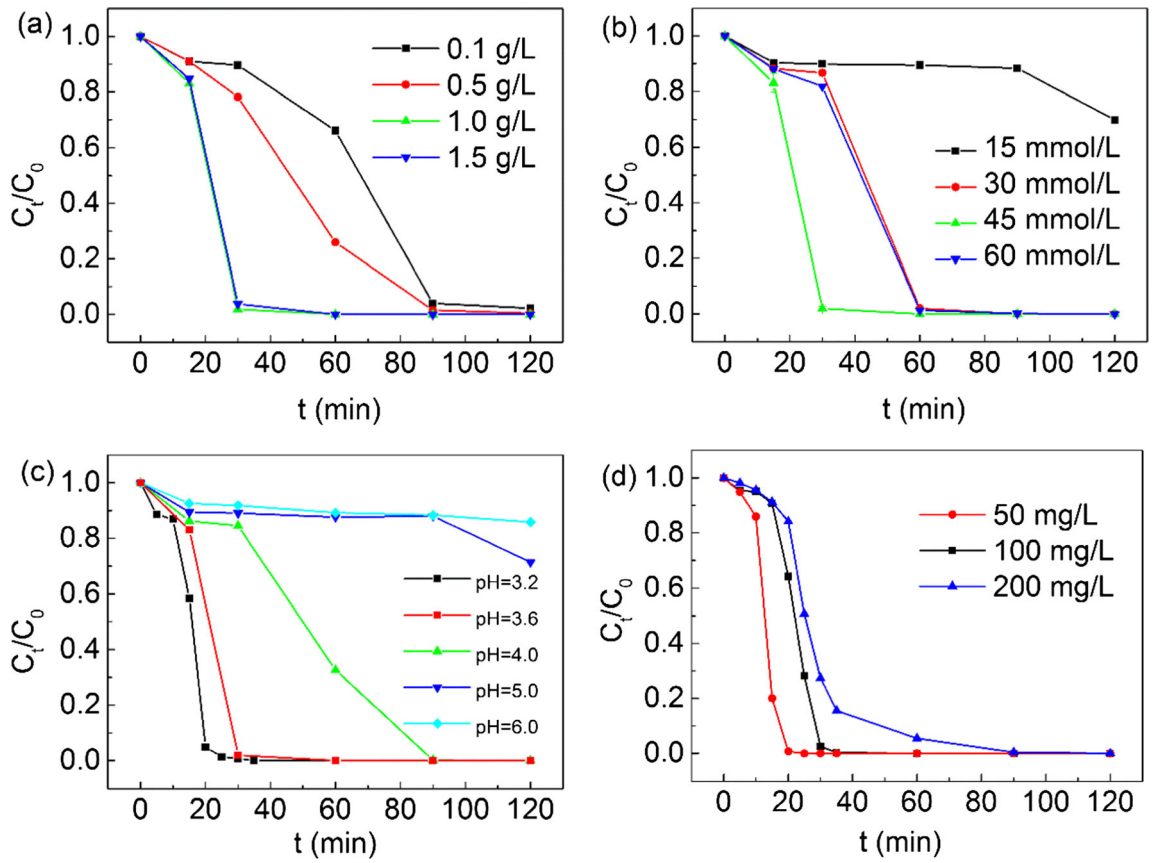

Fig. 9 Effect of operating parameters on phenol degradation using IB-350 as the catalyst: **a** catalyst dosage, **b** H_2O_2 dosage, **c** initial pH, and **d** initial phenol concentration. (Except for the investigated parameters, others were fixed as initial pH = 3.6, 30 °C, 1.0 g/L catalyst, 100 mg/L phenol, and 45 mmol/L H_2O_2)

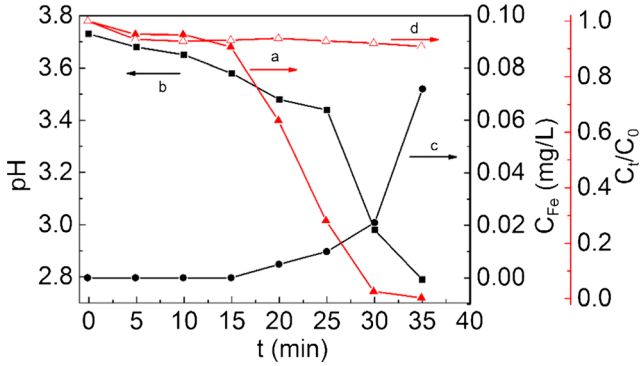

Fig. 10 Changes of phenol (*a*), pH values (*b*), and total Fe ions (*c*) as a function of time using IB-350 as the catalyst (initial pH = 3.6, 30 °C, 1.0 g/L catalyst, 100 mg/L phenol, and 45 mmol/L H_2O_2) and changes of phenol (*d*) in the absence of IB-350 but presence of 0.072 mg/L Fe^{3+} (Other conditions are the same as those in heterogeneous reaction)

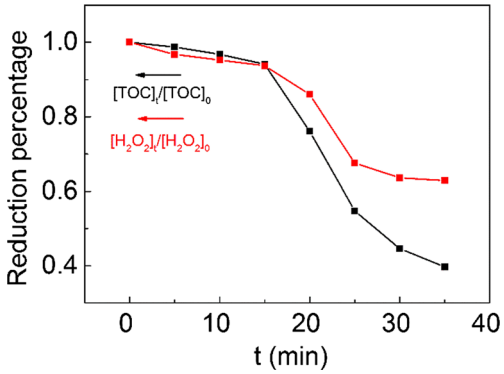

Fig. 12 Changes of H_2O_2 and TOC reduction for phenol degradation using IB-350 as the catalyst (Initial pH = 3.6, 30 °C, 1.0 g/L catalyst, 100 mg/L phenol, and 45 mmol/L H_2O_2)\

35 min reactions, 60.3 % TOC has been reduced, and 37.1 % H_2O_2 has been consumed. The H_2O_2 consumption efficiency (mg TOC/g H_2O_2) can be defined as the amount of TOC converted per unit mass of H_2O_2 decomposed (η) or H_2O_2 fed (ε) (Zazo et al. 2010), which are calculated as 81.4 and 30.2 mg TOC/g H_2O_2, respectively. According to the definition, the efficiency depends on the reaction conditions including reaction time, temperature, initial pH, and catalyst and H_2O_2 dosages. A summary of H_2O_2 consumption efficiency (ε) for organic contaminant removal by using typical magnetic catalysts is shown in Table 2, in which ε was calculated according to the reported TOC reduction and the fed H_2O_2 dosage. Considering the obtained ε in this work is based on the 0.58-h reaction time, the H_2O_2 consumption efficiency of IB-350 is relatively higher as a magnetic catalyst.

Autocatalytic kinetics by intermediates

A notable feature of phenol degradation using IB-350 as the catalyst is the shape of its time evolution (Fig. 8b). The initial kinetics of heterogeneous Fenton-like reaction is very slow, with only 16.9 % phenol removal achieved in the first 15 min. Then, the reaction is significantly accelerated, with the

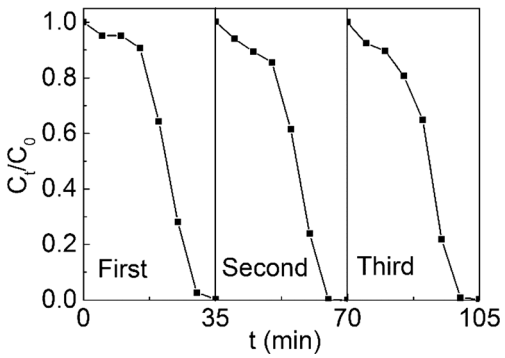

Fig. 11 Reusability of IB-350 in three consecutive tests. (Initial pH = 3.6, 30 °C, 1.0 g/L catalyst, 100 mg/L phenol, and 45 mmol/L H_2O_2)

removal efficiency of phenol increasing sharply to 98.1 % in the next 15 min. Finally, the rate slows down because of the consumption of phenol, and more than 99.7 % phenol has been removed after 35 min reaction. The degradation process can be modeled as two-stage pseudo-first-order kinetics, which has been frequently applied in other heterogeneous Fenton systems (Du et al. 2006; Zhang et al. 2014). The plot of $-\ln(C_t/C_0)$ versus t is shown in Fig. S4. Kinetic constants for the two stages are 0.006 and 0.374 min^{-1}, respectively. The enhancement factor, an index to evaluate the acceleration of degradation, is the ratio of the kinetic constant in the second stage to that in the first stage, which can be calculated as high as 63.3. Similar autocatalysis kinetic of phenol degradation has also been observed in homogeneous Fenton reaction, and the reasons have been attributed to the hydroquinone-like intermediates (Chen and Pignatello 1997; Du et al. 2006).

The main hydroquinone-like intermediates of phenol degradation were investigated via HPLC analyses and shown in Fig. 13. In the first 15 min, concentrations of catechol and hydroquinone increase to 2.22 and 1.77 mg/L, accompanying with 0.65 mg/L benzoquinone. This indicates that in the initial lag period, phenol oxidation by the attack of ·OH is initiated through hydroxylation of the aromatic ring to form catechol and hydroquinone as the mainly products, which are in an equilibrium with benzoquinones. Then, accompanying with the fast phenol degradation in the next 15 min, catechol and hydroquinone only slightly increase, suggesting phenol degradation, ring opening, and chain scission reactions are significantly promoted. Phenol almost disappeared after 35 min reaction, whereas the remaining TOC was 30.2 mg/L. This indicates that the mineralization is not completed, which could be attributed to the refractory intermediates, like oxalic acid in the oxidation reaction (Chen and Pignatello 1997; Zazo et al. 2005).

Since the appearance of intermediates in the lag period causes the significantly enhanced kinetics of phenol degradation, several quinone-like compounds, including hydroquinone, catechol, and benzoquinone, were added into the suspension before the addition of H_2O_2. As shown in Fig. 14, the

Table 2 A comparison of H_2O_2 consumption efficiency (ε) for organic contaminants removal by using magnetic catalysts

Catalyst	Target orange	Operation conditions	Results	Reference
Fe_3O_4 nanoparticles	Phenol	$C_{phenol\text{-}cat\text{-}H2O2}$ = 0.094–5–41 g/L T = 35 °C pH = 7 t = 6 h	X_{phenol} = 100 % X_{TOC} = 43 % ε = 0.76 mg TOC/g H_2O_2	Zhang et al. (2009)
Fe_3O_4 nanoparticles	Phenol	$C_{phenol\text{-}cat\text{-}H2O2}$ = 0.28–0.1–2 g/L T = 40 °C pH = 3 t = 3 h	X_{phenol} = 85 % X_{TOC} = 30 % ε = 31.8 mg TOC/g H_2O_2	Zhang et al. (2008)
Fe_2MnO_4/activated carbon	Methyl orange	$C_{cont\text{-}cat\text{-}H2O2}$ = 0.05–2.5–0.6 g/L T = 30 °C pH = 4 t = 2 h	X_{cont} = 100 % X_{TOC} = 59 % ε = 25.2 mg TOC/g H_2O_2	Nguyen et al. (2011)
Magnetic porous carbon microspheres	Methylene blue	$C_{cont\text{-}cat\text{-}H2O2}$ = 0.04–2-0.54 g/L T = 30 °C pH = 5 t = 0.67 h	X_{cont} = 100 % X_{TOC} = 68 % ε = 25.6 mg TOC/g H_2O_2	Zhou et al. (2014a, b)
Magnetic $CuFe_2O_4$	Imidacloprid	$C_{cont\text{-}cat\text{-}H2O2}$ = 0.01–0.3–1.36 g/L T = 30 °C pH = 3 t = 5 h	X_{cont} = 100 % X_{TOC} = 33 % ε = 1.03 mg TOC/g H_2O_2	Wang et al. (2014)
Magnetite/MCM-41	Methylene blue	$C_{cont\text{-}cat\text{-}H2O2}$ = 0.05–10–3.3 g/L T = 25 °C pH = natural t = 3 h	X_{cont} = 50 % X_{TOC} = 43 % ε = 3.9 mg TOC/g H_2O_2	Nogueira et al. (2014)
IB-350	Phenol	$C_{cont\text{-}cat\text{-}H2O2}$ = 0.1–1–1.53 g/L T = 30 °C pH = 3.6 t = 0.58 h	X_{cont} = 99 % X_{TOC} = 60.3 % ε = 30.2 mg TOC/g H_2O_2	This work

lag periods in the profiles of phenol time evolution disappear in the presence of hydroquinone or catechol, while they do not change in the presence of benzoquinone. The former two additives greatly accelerate phenol degradation. Phenol reduction after only 5 min reactions can reach 49.6 and 50.4 % for the addition of hydroquinone or catechol, respectively. The catalytic behavior of hydroquinone or catechol in the heterogeneous reaction can be attributed to the enhanced ·OH production through promoting the transformation of ≡Fe(III) into ≡Fe(II) according to the Eq. (4). This can be rationalized by their reduction potentials, which are 0.77 and 0.31 V for Fe^{3+} and hydroquinone, respectively (Wardman 1989). Therefore, the produced hydroquinone or catechol during phenol degradation would promote the formation of ≡Fe(II) in the catalyst, as well as the generation of ·OH according to the reaction shown in Eq. (3), and accordingly result in an autocatalytic kinetic for phenol removal. It can be expected that addition of such compounds could also be an alternative way to improve the removal efficiency of organic pollutant in heterogeneous Fenton-like reactions.

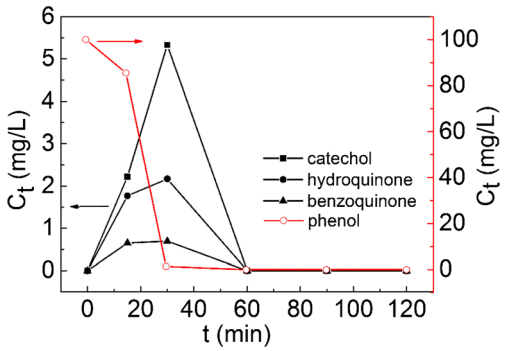

Fig. 13 Evolution of typical intermediates in phenol degradation using IB-350 as the catalyst. (Initial pH = 3.6, 30 °C, 1.0 g/L catalyst, 100 mg/L phenol, and 45 mmol/L H_2O_2)

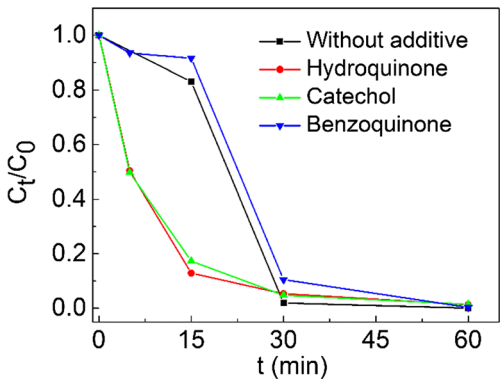

Fig. 14 Phenol degradation using IB-350 as the catalyst in the absence or presence of 1.06 mmol/L hydroquinone-like compounds. (Initial pH = 3.6, 30 °C, 1.0 g/L catalyst, 100 mg/L phenol, and 45 mmol/L H_2O_2)

(4)

Conclusion

An efficient magnetically separable catalyst, maghemite/montmorillonite composite, has been synthesized by coprecipitation of iron precursors onto montmorillonite K10 and followed with calcinations. The presence of MK10 inhibits the growth of maghemite nanoparticles and the phase transition of γ-Fe_2O_3 into α-Fe_2O_3 and accordingly makes the composite retaining the excellent magnetic property after calcined at even 450 °C for 24 h. The sample calcined at 350 °C displays the highest catalytic activity, achieving more than 99 % phenol reduction after only 35 min reaction at pH 3.6. The enhanced catalytic activity after calcinations can be attributed to the negatively charged surface and the strengthened interaction between iron and aluminosilicate frameworks. In the heterogeneous system, hydroquinone-like intermediates from phenol degradation result in an autocatalytic kinetic. The composite displays high catalytic activity and stability, low iron leaching, and can be conveniently separated by an external magnetic field for recycle applications. This work offers a promising strategy to develop efficient magnetic catalysts by the incorporation of clays with aluminosilicate frameworks.

Acknowledgments Financial supports from the Natural Science Foundation of China (21377084) and Special Fund for Agro-scientific Research in the Public Interest in China (201503107) are gratefully acknowledged. We also acknowledge the support and valuable suggestion in zeta potential measurements from Ms. Xiaojuan Yu of School of Environmental Science and Engineering, Shanghai Jiao Tong University.

References

Bruce W, Meek ME, Newhook R (2001) Phenol: hazard characterization and exposure–response analysis. J Environ Sci Health, Part C 19: 305–324

Cao KZ, Jiao LF, Liu HQ, Liu YC, Wang YJ, Guo ZP, Yuan HT (2015) 3D hierarchical porous α-Fe_2O_3 nanosheets for high-performance lithium-ion batteries. Adv Energy Mater 5:1401421

Chae HJ, Nam I-S, Ham SW, Hong SB (2001) Physicochemical characteristics of pillared interlayered clays. Catal Today 68:31–40

Chen RZ, Pignatello JJ (1997) Role of quinone intermediates as electron shuttles in Fenton and photoassisted Fenton oxidations of aromatic compounds. Environ Sci Technol 31:2399–2406

Chen JX, Zhu LZ (2007) Heterogeneous UV-Fenton catalytic degradation of dyestuff in water with hydroxyl-Fe pillared bentonite. Catal Today 126:463–470

Chen JX, Zhu LZ (2011) Oxalate enhanced mechanism of hydroxyl-Fe-pillared bentonite during the degradation of Orange II by UV-Fenton process. J Hazard Mater 185:1477–1481

Chen QQ, Wu PX, Dang Z, Zhu NW, Li P, Wu JH, Wang XD (2010) Iron pillared vermiculite as a heterogeneous photo-Fenton catalyst for photocatalytic degradation of azo dye reactive brilliant orange X-GN. Sep Purif Technol 71:315–323

Djeffal L, Abderrahmane S, Benzina M, Fourmentin M, Siffert S, Fourmentin S (2014) Efficient degradation of phenol using natural clay as heterogeneous Fenton-like catalyst. Environ Sci Pollut Res 21:3331–3338

Du YX, Zhou MH, Lei LC (2006) Role of the intermediates in the degradation of phenolic compounds by Fenton-like process. J Hazard Mater 136:859–865

Feng JY, Hu XJ, Yue PL (2004) Novel bentonite clay-based Fe-nanocomposite as a heterogeneous catalyst for photo-Fenton discoloration and mineralization of orange II. Environ Sci Technol 38:269–275

Feng JY, Hu XJ, Yue PL (2006) Effect of initial solution pH on the degradation of Orange II using clay-based Fe nanocomposites as heterogeneous photo-Fenton catalyst. Water Res 40:641–646

Gao JN, Ran XZ, Shi CM, Cheng HM, Cheng TM, Su YP (2013) One-step solvothermal synthesis of highly water-soluble, negatively charged superparamagnetic Fe_3O_4 colloidal nanocrystal clusters. Nanoscale 5:7026–7033

Garrido-Ramirez EG, Theng BKG, Mora ML (2010) Clays and oxide minerals as catalysts and nanocatalysts in Fenton-like reactions—a review. Appl Clay Sci 47:182–192

Grosvenor AP, Kobe BA, Biesinger MC, McIntyre NS (2004) Investigation of multiplet splitting of Fe 2p XPS spectra and bonding in iron compounds. Surf Interface Anal 36:1564–1574

Herrero E, Cabañas MV, Vallet-Regí M, Martínez JL, González-Calbet JM (1997) Influence of synthesis conditions on the γ-Fe_2O_3 properties. Solid State Ionics 101–103:213–219

Iurascu B, Siminiceanu I, Vione D, Vicente MA, Gil A (2009) Phenol degradation in water through a heterogeneous photo-Fenton process catalyzed by Fe-treated laponite. Water Res 43:1313–1322

Jiang WQ, Yang HC, Yang SY, Horng HE, Hung JC, Chen YC, Hong C-Y (2004) Preparation and properties of superparamagnetic nanoparticles with narrow size distribution and biocompatible. J Magn Magn Mater 283:210–214

Kalidasan V, Liu XL, Herng TS, Yang Y, Ding J (2016) Bovine serum albumin-conjugated ferrimagnetic iron oxide nanoparticles to enhance the biocompatibility and magnetic hyperthermia performance. Nano-Micro Lett 8:80–93

Li W, Wan D, Wang G, Chen K, Hu Q, Lu L (2016) Heterogeneous Fenton degradation of Orange II by immobilization of Fe_3O_4 nanoparticles onto Al-Fe pillared bentonite. Korean J Chem Engin 33: 1557–1564

Lin SS, Gurol MD (1998) Catalytic decomposition of hydrogen peroxide on iron oxide: kinetics, mechanism, and implications. Environ Sci Technol 32:1417–1423

Ling YH, Long MC, Hu PD, Chen Y, Huang JW (2014) Magnetically separable core-shell structural γ-Fe_2O_3@Cu/Al-MCM-41 nanocomposite and its performance in heterogeneous Fenton catalysis. J Hazard Mater 264:195–202

Lou ZC, Zhou ZW, Zhang W, Zhang XH, Hu XD, Liu PD, Zhang HQ (2015) Magnetized bentonite by Fe_3O_4 nanoparticles treated as adsorbent for methylene blue removal from aqueous solution:

synthesis, characterization, mechanism, kinetics and regeneration. J Taiwan Inst Chem Eng 49:199–205

Machala L, Tucek J, Zboril R (2011) Polymorphous transformations of nanometric iron(III) oxide: a review. Chem Mater 23:3255–3272

Munoz M, de Pedro ZM, Casas JA, Rodriguez JJ (2015) Preparation of magnetite-based catalysts and their application in heterogeneous Fenton oxidation—a review. Appl Catal B-Environ 176:249–265

Nguyen TD, Phan NH, Do MH, Ngo KT (2011) Magnetic Fe_2MO_4 (M: Fe, Mn) activated carbons: fabrication, characterization and heterogeneous Fenton oxidation of methyl orange. J Hazard Mater 185: 653–661

Nogueira RF, Oliveira MC, Paterlini WC (2005) Simple and fast spectrophotometric determination of H_2O_2 in photo-Fenton reactions using metavanadate. Talanta 66:86–91

Nogueira AE, Castro IA, Giroto AS, Magriotis ZM (2014) Heterogeneous Fenton-like catalytic removal of methylene blue dye in water using magnetic nanocomposite (MCM-41/magnetite). J Catalysts:1–6

Oliveira LCA, Fabris JD, Pereira MC (2012) Iron oxides and their applications in catalytic processes: a review. Quim Nov. 36:123–130

Orolinova Z, Mockovciakova A, Zelenak V, Myndyk M (2012) Influence of heat treatment on phase transformation of clay-iron oxide composite. J Alloy Compd 511:63–69

Pham AL-T, Lee C, Doyle FM, Sedlak DL (2009) A silica-supported iron oxide catalyst capable of activating hydrogen peroxide at neutral pH values. Environ Sci Technol 43:8930–8935

Qin YL, Long MC, Tan BH, Zhou BX (2014) RhB adsorption performance of magnetic adsorbent Fe_3O_4/RGO composite and its regeneration through a Fenton-like reaction. Nano-Micro Lett 6:125–135

Sanders JP, Gallagher PK (2003) Kinetics of the oxidation of magnetite using simultaneous TG/DSC. J Therm Anal Calorim 72:777–789

Sarikaya Y, Önal M, Baran B, Alemdaroğlu T (2000) The effect of thermal treatment on some of the physiochemical properties of a bentonite. Clay Clay Miner 48:557–562

Schimanke G, Martin M (2000) In situ XRD study of the phase transition of nanocrystalline maghemite (γ-Fe_2O_3) to hematite (α-Fe_2O_3). Solid State Ionics 136–137:1235–1240

Tamura H, Goto K, Yotsuyanagi T, Nagayama M (1974) Spectrophotometric determination of iron(II) with 1,10-phenanthroline in the presence of large amounts of iron(III). Talanta 21:314–318

Tireli AA, Guimarães dIR, Terra JCS, da Silva RR, Guerreiro MC (2015) Fenton-like processes and adsorption using iron oxide-pillared clay with magnetic properties for organic compound mitigation. Environ Sci Pollut Res 22:870–881

Usman M, Faure P, Ruby C, Hanna K (2012) Remediation of PAH-contaminated soils by magnetite catalyzed Fenton-like oxidation. Appl Catal B-Environ 117:10–17

Usman M, Faure P, Lorgeoux C, Ruby C, Hanna K (2013) Treatment of hydrocarbon contamination under flow through conditions by using magnetite catalyzed chemical oxidation. Environ Sci Pollut Res 20: 22–30

Virkutyte J, Varma RS (2014) Eco-friendly magnetic iron oxide-pillared montmorillonite for advanced catalytic degradation of dichlorophenol. ACS Sustain Chem Eng 2:1545–1550

Walling C, Goosen A (1973) Mechanism of the ferric ion catalyzed decomposition of hydrogen peroxide. Effect of organic substrates. J Am Chem Soc 95:2987–2991

Wan D, Li W, Wang G, Chen K, Lu L, Hu Q (2015) Adsorption and heterogeneous degradation of rhodamine B on the surface of magnetic bentonite material. Appl Surf Sci 349:988–996

Wang YB, Zhao HY, Li MF, Fan JQ, Zhao GH (2014) Magnetic ordered mesoporous copper ferrite as a heterogeneous Fenton catalyst for the degradation of imidacloprid. Appl Catal B-Environ 147:534–545

Wang XQ, Zhang HR, Jing HJ, Cui LQ (2015) Highly efficient labeling of human lung cancer cells using cationic poly-l-lysine-assisted magnetic iron oxide nanoparticles. Nano-Micro Lett 7:374–384

Wardman P (1989) Reduction potentials of one-electron couples involving free radicals in aqueous solution. J Phys Chem Ref Data 18: 1637–1755

Xia M, Chen C, Long MC, Chen C, Cai WM, Zhou BX (2011a) Magnetically separable mesoporous silica nanocomposite and its application in Fenton catalysis. Micropor Mesopor Mat 145:217–223

Xia M, Long MC, Yang YD, Chen C, Cai WM, Zhou BX (2011b) A highly active bimetallic oxides catalyst supported on Al-containing MCM-41 for Fenton oxidation of phenol solution. Appl Catal B-Environ 110:118–125

Xu L, Wang J (2011) A heterogeneous Fenton-like system with nanoparticulate zero-valent iron for removal of 4-chloro-3-methyl phenol. J Hazardous Mater 186:256–264

Yamashita T, Hayes P (2008) Analysis of XPS spectra of Fe^{2+} and Fe^{3+} ions in oxide materials. Appl Surf Sci 254:2441–2449

Yu LL, Wu H, Wu BN, Wang ZY, Cao HM, Fu CY, Jia NQ (2014) Magnetic Fe_3O_4-reduced graphene oxide nanocomposites-based electrochemical biosensing. Nano-Micro Lett 6:258–267

Yu L, Yang X, Ye Y, Wang D (2015) Efficient removal of atrazine in water with a Fe_3O_4/MWCNTs nanocomposite as a heterogeneous Fenton-like catalyst. RSC Adv 5:46059–46066

Zazo JA, Casas JA, Mohedano AF, Gilarranz MA, Rodríguez JJ (2005) Chemical pathway and kinetics of phenol oxidation by Fenton's reagent. Environ Sci Technol 39:9295–9302

Zazo JA, Pliego G, Blasco S, Casas JA, Rodriguez JJ (2010) Intensification of the Fenton process by increasing the temperature. Ind Eng Chem Res 50:866–870

Zhang JB, Zhuang J, Gao LZ, Zhang Y, Gu N, Feng J, Yang DL, Zhu JD, Yan XY (2008) Decomposing phenol by the hidden talent of ferromagnetic nanoparticles. Chemosphere 73:1524–1528

Zhang SX, Zhao XL, Niu HY, Shi YL, Cai YQ, Jiang GB (2009) Superparamagnetic Fe_3O_4 nanoparticles as catalysts for the catalytic oxidation of phenolic and aniline compounds. J Hazard Mater 167: 560–566

Zhang GK, Gao YY, Zhang YL, Guo YD (2010) Fe_2O_3-pillared rectorite as an efficient and stable Fenton-like heterogeneous catalyst for photodegradation of organic contaminants. Environ Sci Technol 44:6384–6389

Zhang L, Zeng H, Zeng Y, Zhang Z, Zhao X (2014) Heterogeneous Fenton-like degradation of 4-chlorophenol using a novel FeIII-containing polyoxometalate as the catalyst. J Mol Catal A Chem 392:202–207

Zhang H, Liang X, Yang C, Niu C, Wang J, Su X (2016) Nano γ-Fe_2O_3/bentonite magnetic composites: synthesis, characterization and application as adsorbents. J Alloys Compds 688:1019–1027

Zhou LC, Shao YM, Liu JR, Ye ZF, Zhang H, Ma JJ, Jia Y, Gao WJ, Li YF (2014a) Preparation and characterization of magnetic porous carbon microspheres for removal of methylene blue by a heterogeneous Fenton reaction. ACS Appl Mater Inter 6:7275–7285

Zhou LC, Zhang H, Ji LQ, Shao YM, Li YF (2014b) Fe_3O_4/MWCNT as a heterogeneous Fenton catalyst: degradation pathways of tetrabromobisphenol A. RSC Adv 4:24900–24908